

Trifluoromethyl-Substituted Conjugated Oligoelectrolytes

Yan Ren^[a, b] and Guillermo C. Bazan^{*[a]}

Abstract: Conjugated oligoelectrolytes (COEs) are being introduced into a variety of optical and electronic technologies, yet the dependence of their properties as a function of molecular structure remains poorly understood. In response, we designed, synthesized, and examined a new tetracationic COE, namely, 1,4-bis[9',9'-bis[6''-(*N,N,N*-trimethylammonium)hexyl]-2'-fluorenyl]-2,5-bis(trifluoromethyl)benzene tetrabromide (FPF-F6), which contains bulky electron-withdrawing trifluoromethyl groups, and compared its properties with the unsubstituted counterpart 1,4-bis[9',9'-bis[6''-(*N,N,N*-trime-

thylammonium)hexyl]-2'-fluorenyl}benzene tetrabromide (FPF). The ground-state geometry of FPF-F6 is primarily twisted with little electronic communication between the aromatic units, as confirmed by single-crystal X-ray diffraction studies of the neutral precursor. However, absorption and photoluminescence spectroscopies reveal that the excited state of FPF-F6 displays strong intramolecular charge-transfer

Keywords: biosensors • charge transfer • conjugation • oligoelectrolytes • photoluminescence

characteristics. Solution AFM in aqueous media shows that introduction of trifluoromethyl groups changes the size and aspect ratio of supramolecular aggregates that are brought together as a result of hydrophobic interactions. Furthermore, addition of ssDNA to FPF-F6 leads to interoligoelectrolyte complexes wherein the backbone is more planar; the environment the chromophore experiences under these conditions is also considerably less polar. These findings provide considerable insight into the complex photophysics of electronically conjugated materials in aqueous media.

Introduction


Conjugated oligoelectrolytes (COEs) contain a well-defined number of π -delocalized repeat units with pendant functional groups capable of being ionized in high dielectric media.^[1] These molecules are becoming incorporated into a range of innovative technologies that require light-harvesting capabil-

ities or mediation of charge-carrier injection/transport. For example, cationic COEs can be complexed with (anionic) dye-labeled single-stranded DNA (ssDNA) in aqueous media.^[2] The resulting electrostatic aggregates contain structural features that allow for differential interactions with various proteins and optical properties that change in response to these structural/local site modifications. As a result, it is possible by using various ssDNA sequences to create an array of aggregates that can identify various proteins without relying on lock-and-key principles. A thin COE layer can also be introduced adjacent to a metallic electrode to lower the barrier to electron injection into an organic semiconductor.^[1,3] This process requires preferential alignment of dipoles and involves surface reconstruction processes in the bulk that remain poorly understood.^[4]

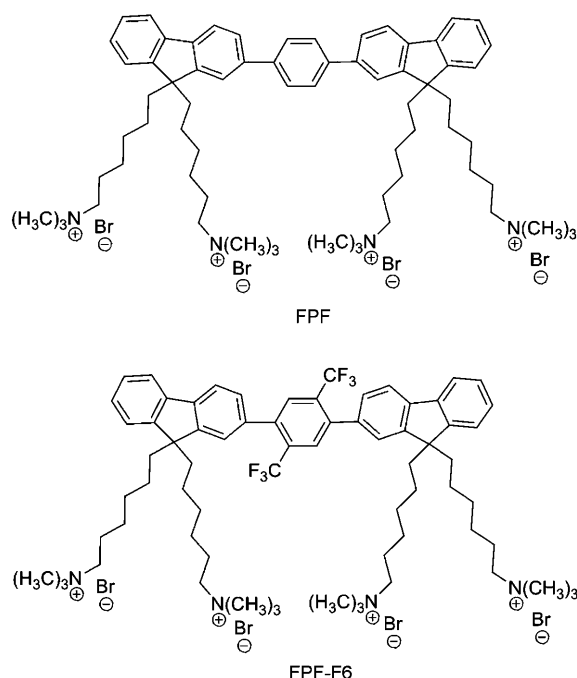
Despite the progress in applying COEs to various technologies, there have been only a few studies on how their molecular structure influences intrinsic optical properties under various conditions and in different media. Conjugated polyelectrolytes, that is, COE analogues with a larger number of repeat units along the backbone, have been examined more broadly.^[5] These studies have raised awareness for processes that are strongly influenced by interchain contacts and by different chemical functionalities.^[6] Such features are a spe-

[a] Dr. Y. Ren, Prof. G. C. Bazan
Departments of Materials and Chemistry & Biochemistry
Center for Polymers and Organic Solids
University of California, Santa Barbara, California 93106 (USA)
Fax: (+1) 805-893-4270
E-mail: bazan@chem.ucsb.edu

[b] Dr. Y. Ren
State Key Laboratory of Crystal Materials
Shandong University, Jinan 250100 (P. R. China)

 Supporting information for this article is available on the WWW under <http://dx.doi.org/10.1002/chem.201000885>. It contains crystal data, structure refinement, and full analysis of intermolecular interactions in lattice for p-FPF and p-FPF-F6. UV absorption and photoluminescence (PL) spectra of FPF-F6 in water, PL spectrum of FPF/DNA complex.

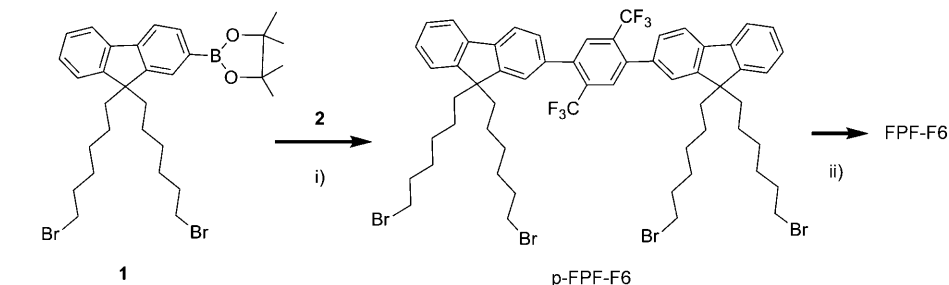
cial concern in water, where the hydrophobic aromatic π -delocalized backbone provides the driving force for spontaneous aggregation, even in the absence of an oppositely charged polyelectrolyte.^[7] In response to the absence of basic information on COE photophysics, supramolecular structures,^[8] and aggregation tendencies, we examine in this contribution 1,4-bis[9',9'-bis[6''-(*N,N,N*-trimethylammonium)-hexyl]-2'-fluorenyl]benzene tetrabromide (FPF) and 1,4-bis[9',9'-bis[6''-(*N,N,N*-trimethylammonium)hexyl]-2'-fluorenyl]-2,5-bis(trifluoromethyl)benzene tetrabromide (FPF-F6), with the goal of understanding the influence of attaching a bulky electron withdrawing group to the conjugated segment.



Herein, we describe the synthesis of FPF-F6 and subsequently show spectral features associated with structural distortions of the backbone and intramolecular charge-transfer characteristics that stem from the electron-withdrawing trifluoromethyl groups. Single-crystal X-ray diffraction experiments of precursor materials are used to support evidence of the conformational differences between FPF and FPF-F6. Finally, we report the differences in the aggregation of these COEs, both spontaneously as a report of hydrophobic interactions, and upon electrostatic binding to an oppositely charged macromolecule.

Results and Discussion

Syntheses and characterization: Compound FPF was synthesized according to a procedure reported previously.^[9] The synthesis of FPF-F6 is shown in Scheme 1. Treatment of 2-



Scheme 1. Synthesis of FPF-F6: i) 2,5-dibromo-1,4-bis(trifluoromethyl)benzene (**2**), [Pd(PPh₃)₄], K₂CO₃, toluene, 95 °C; ii) NMe₃, THF, methanol, –78 °C.

bromo-9,9-bis(6'-bromohexyl)fluorene^[10] with bis(pinacolato)diboron under air-free conditions provided 2-(4,4,5,5-tetramethyl[1,3,2]dioxaborolane)-9,9-bis(6'-bromohexyl)fluorene (**1**). Bromination of 1,4-bis(trifluoromethyl)benzene was achieved by using trifluoroacetic acid (TFA) as the solvent in the presence of catalytic H₂SO₄ to give 2,5-dibromo-1,4-bis(trifluoromethyl)benzene (**2**) in 90 % yield. The following step was a Suzuki cross-coupling reaction between compounds **1** and **2** to provide the neutral precursor oligomer 1,4-bis(9',9'-bis(6''-bromohexyl)-2'-fluorenyl)-2,5-bis(trifluoromethyl)benzene (p-FPF-F6, in Scheme 1). Characterization of p-FPF-F6 was accomplished by mass spectrometry by using FAB/NBA as well as ¹H and ¹³C NMR spectroscopy and elemental analysis. The *m/z* signals observed in the range from 1190 to 1198 are consistent with the correct isotopic distribution due to four bromide atoms. In the last step, compound p-FPF-F6 was quaternized by using NMe₃ in a THF/MeOH solvent mixture to yield FPF-F6, which exhibits good solubility in aqueous media and highly polar organic solvents.

The composition of FPF-F6 was confirmed by NMR spectroscopy and ESI-MS. Compared with the ¹H NMR spectrum of the neutral p-FPF-F6, a singlet appears at δ = 3.06 ppm for FPF-F6, with an integrated area that coincides with the anticipated number of protons from four trimethylammonium groups. In the ¹³C NMR spectrum of FPF-F6, the occurrence of a peak at δ = 56.2 ppm with highest intensity among all the alkyl resonances is consistent with quaternization by trimethylamine. At the same time, the chemical shift of the terminal carbon in the pendant alkyl group moves to higher field (δ = 59.1 ppm) owing to the action of the adjacent nitrogen-based cation. ESI-MS supports the proposed structure: the quasimolecular ion peak *m/z* is 277.67 [M–4Br]⁺. Thermogravimetric analysis (TGA) revealed that FPF-F6 is highly hydroscopic.^[11] After standing in air for an extended period of time one finds up to seven adsorbed water molecules per conjugated segment. TGA

also showed that the content of the water absorbed in the powder is variable based on the duration of storage.

Absorption and photoluminescence spectroscopy: Figure 1 compares the UV/Vis and photoluminescence (PL) spectra of FPF and FPF-F6 in phosphate buffer. This aqueous

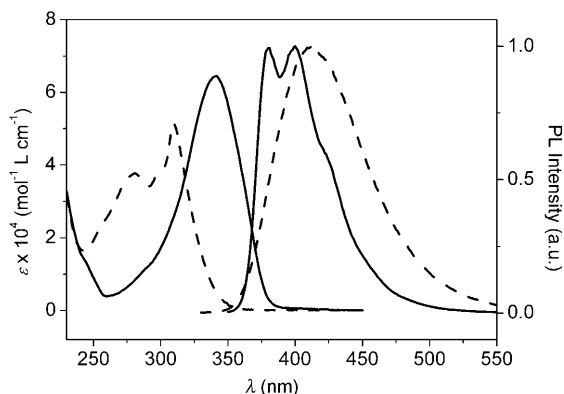


Figure 1. Absorption and PL spectra of FPF (solid) and FPF-F6 (dashed) in phosphate buffer.

medium was of specific interest to us because of its relevance to conditions usually found in biosensory schemes. However, spectral features observed in buffer are essentially identical to those observed in water (see the Supporting Information). We begin by noting that the absorption maximum (λ_{max}) of FPF, which lacks the two trifluoromethyl groups, is observed at 340 nm. Using an excitation wavelength (λ_{ex}) of 340 nm leads to a vibrationally defined emission band with a maximum (λ_{em}) at 380 nm, corresponding to a Stokes shift of 40 nm (0.39 eV). Examination of the absorption spectrum of FPF-F6 reveals that $\lambda_{\text{max}}=310$ nm, which is considerably blueshifted relative to that of FPF. The spectral characteristics of the FPF-F6 absorption are also considerably sharper and with more fine structure. The PL spectrum of FPF-F6 is broad with $\lambda_{\text{em}}=413$ nm, corresponding to a Stokes shift of 103 nm (1.0 eV). The PL quantum yields of FPF and FPF-F6 in phosphate buffer with quinine sulfate as the standard are 0.85 and 0.72, respectively. Understanding the differences in spectral properties, particularly the absorbance between FPF and FPF-F6, guides the choice of subsequent experiments.

We next focused on possible perturbations as a result of the ionic functionalities. Figure 2 shows that the absorption spectra of FPF-F6 and the precursor oligomer p-FPF-F6 in DMF are nearly indistinguishable. DMF was chosen because sufficient quantities of the neutral and charged versions of the chromophores can be dissolved in this solvent. It is helpful to note here that the absorption spectra of FPF-F6 in DMF and aqueous media are very similar to each other. Figure 2 also shows that the absorption spectra of FPF-F6 and p-FPF-F6 resemble that of compound **1** (Scheme 1), which corresponds to a well-defined fluorene chromophore. However, the PL of **1** is blueshifted relative to that of FPF-

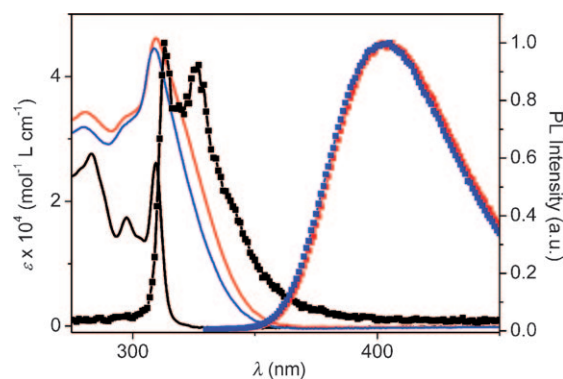
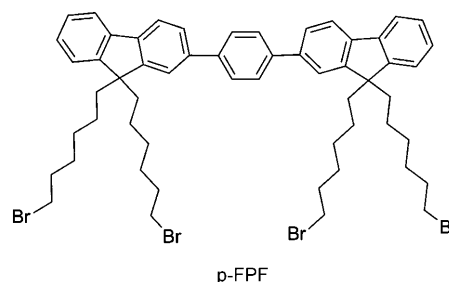


Figure 2. Absorption (line) and PL (square) spectra of **1** (black), p-FPF-F6 (red), and FPF-F6 (blue) in DMF.

F6 in the same solvent (DMF). We surmise that neither the solvent nor the presence of adjacent charged groups influence the absorption spectrum of the integral π component in FPF-F6. Furthermore, despite the apparently more extended conjugation length, the absorption of FPF-F6 behaves similar to that of a single fluorene fragment. These data suggest ineffective delocalization in the ground state and would be consistent with the aromatic rings in the fluorene–phenylene–fluorene framework being severely twisted relative to each other.

Solvatochromic effects on the PL properties of the chromophores were explored by taking advantage of the neutral precursors. According to previous studies on neutral and charged distyrylbenzene derivatives, ionic groups on the periphery of the molecular structure do not greatly perturb the excited-state energies.^[12] Rather, their function is to increase solubility in polar media. As a result, the PL properties of neutral and charged chromophores are very close to each other when in the same solvent. This effect has already been demonstrated in Figure 2. Hexane and DMSO were used for the solvatochromic studies described herein, since the precursor to FPF, 1,4-bis[9', 9'-bis(6''-bromohexyl)-2'-fluorenyl]benzene (p-FPF) and p-FPF-F6 possess acceptable solubility in these solvents.



As shown in Figure 3, the PL maxima of p-FPF-F6 red-shifts from $\lambda_{\text{em}}=376$ nm in hexane to $\lambda_{\text{em}}=405$ nm in DMSO, corresponding to a solvatochromic shift of 29 nm (≈ 0.24 eV). In the case of p-FPF the shift is much less pro-

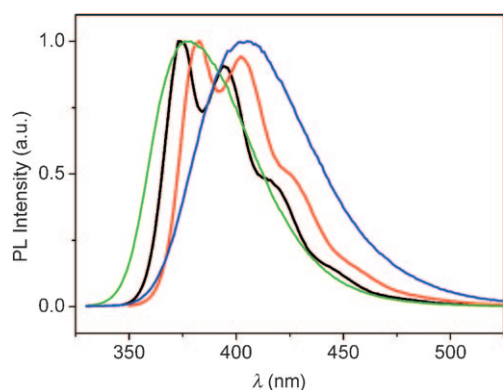


Figure 3. Solvent effects on the PL spectra of p-FPF in hexane (black) and DMSO (red); p-FPF-F6 in hexane (green), and DMSO (blue), [p-FPF] = [p-FPF-F6] = 5 μ M, λ_{ex} (p-FPF) = 340 nm, λ_{ex} (p-FPF-F6) = 310 nm.

nounced, in the order of 9 nm (≈ 0.08 eV). Larger solvatochromic shifts and broader spectra are observed for molecules with more polar excited states.^[13] This observation arises due to the ability of the solvent to lower the chromophore energy through Coulomb-type interactions between the solvent dipole and the electrostatic distribution in the excited state.^[14] The larger solvatochromic effect observed with p-FPF-F6 than p-FPF indicates that introduction of the trifluoromethyl groups leads to a more polar excited state. This observation, in conjunction with the more redshifted emission, leads us to propose that p-FPF-F6, and by inference that of FPF-F6, has a more planar geometry in the excited than in the ground state. Under these conditions, the influence of the electron-rich terminal rings is more pronounced and leads to an excited state with intermolecular charge-transfer (ICT) characteristics. In the case of FPF, regardless of the preferred conformation, there is a much weaker driving force for ICT, the excitation is primarily described by a π - π^* transition.

Low-temperature PL measurements were performed to obtain additional insight into the role of the solvent. One particular interesting challenge is to untangle how intramolecular planarization and solvent reorganization processes contribute to differences in spectral characteristics. To decrease the solvent relaxation as much as possible at low temperature, we measured the PL of FPF and FPF-F6 in the polar solvent ethylene glycol, the viscosity of which increases gradually with decreasing temperature and does not crystallize.^[14,15] The PL spectra obtained with FPF and FPF-F6 in ethylene glycol at 77 and 293 K are shown in Figures 4 and 5, respectively. From Figure 4, one observes little difference between the PL maxima of FPF at 293 and 77 K (5 nm blueshift upon decreasing the temperature, 0.04 eV). In contrast, there is 20 nm (0.17 eV) blueshift for FPF-F6 at 77 K (Figure 5). Furthermore, note that the PL spectrum of FPF-F6 at low temperature ($\lambda_{\text{em}} = 370$ nm) is blueshifted from that of FPF at room temperature ($\lambda_{\text{em}} = 380$ nm), which is opposite to the case at room temperature (see Figure 1). It is also informative to compare the PL spectrum of FPF-F6 in ethylene glycol at 77 K with p-FPF-F6 in hexane at room

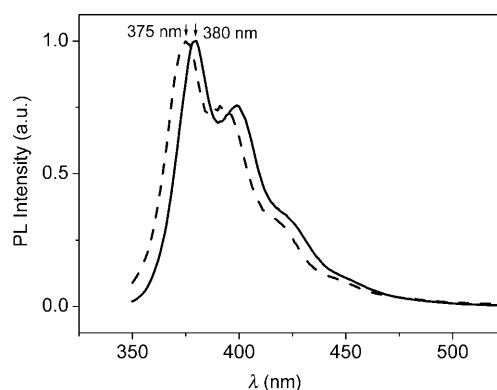


Figure 4. PL spectra of FPF in ethylene glycol at 293 (solid line) and 77 K (dashed line).

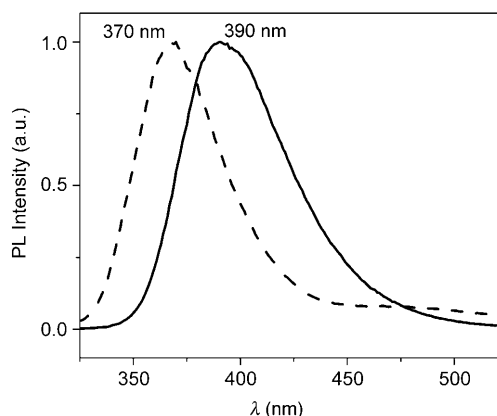


Figure 5. PL spectra of FPF-F6 in ethylene glycol at 293 (solid line) and 77 K (dashed line).

temperature (Figure 3), where solvent stabilization by dipole interactions is anticipated to be minimal. The PL spectrum at low temperature is about 3–6 nm blueshifted from that at room temperature in hexane. Although not quantitative in nature, the collective set of observations described above indicates that the viscous environment of ethylene glycol at 77 K not only slows down the rate of solvent reorganization to stabilize the more polar excited state, but also partially decreases the rate of inter-ring rotation, leading to less effective electronic delocalization.

Single-crystal X-ray diffraction studies: Single crystals of FPF and FPF-F6 suitable for X-ray diffraction studies proved difficult to obtain. Both species form highly viscous saturated solutions in polar solvents such as methanol. However, the situation is different for the precursor molecules. Single crystals of p-FPF and p-FPF-F6 were grown by slow evaporation of solutions in hexane at room temperature. Figure 6 shows the molecular structures determined by X-ray diffraction (complete details concerning crystal data and structural refinements are provided in the Supporting Information). Both p-FPF and p-FPF-F6 crystallize in a triclinic lattice with the space group $P\bar{1}$. The two fluorene rings in

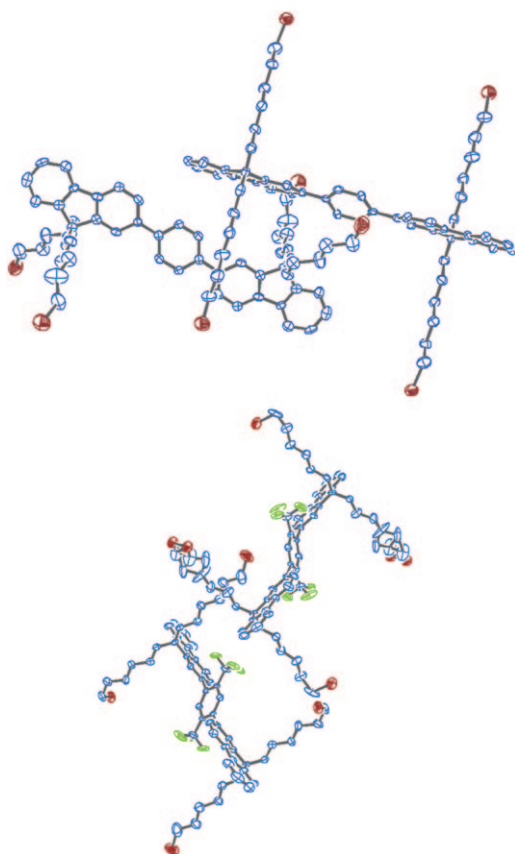


Figure 6. Molecular structures of p-FPF and p-FPF-F6. The hydrogen atoms are omitted for improving the clarity of the molecular features. (blue: C, red: Br, green: F)

the molecules are parallel to each other. Their pendant groups situate perpendicular to the fluorene planes. However, p-FPF and p-FPF-F6 exhibit different torsion angles between the internal ring and the outer fluorene planes. For the two independent molecules in the unit cell of p-FPF, the torsion angles are similar to each other with values of $-26.5(8)$ and $-27.5(8)^\circ$. In contrast, for p-FPF-F6, the torsion angles of the trifluoromethyl-substituted benzene plane to the fluorene ring are different in the two independent molecules: $72.7(10)$ and $-58.2(11)^\circ$, which are much larger than the torsion angles in p-FPF. These details are fully in agreement with the assignment of the more blueshifted absorption in FPF-F6 (Figure 1) due to less effective electronic delocalization in the ground state.

Examination of the lattice diagrams (see the Supporting Information) shows close intermolecular contacts in the case of p-FPF. For example, face-to-face contact between symmetric molecules along the π -stacking direction is 3.27 \AA . Introduction of the trifluoromethyl groups leads to a considerable weakening of the interaction between aromatic units. A full analysis can be found in the Supporting Information.

Liquid-phase AFM images of aggregates: Aggregation of COEs and related molecules in aqueous media as a result of

the hydrophobic aromatic framework is known to play an important role in determining the optical performance of optically amplified fluorescent biosensory assays.^[16] This body of work led us to investigate, by using liquid phase AFM,^[17] to what degree differences in the molecular structures of FPF-F6 and FPF might change the sizes and aspect ratios of the multichromophore aggregates. Compared with traditional AFM, liquid-phase AFM can produce high-resolution topographic images of supramolecular assemblies in solution upon adsorption onto a negatively charge mica surface.

A typical liquid AFM experiment follows the deposition of $50 \mu\text{L}$ of COE solution at a concentration of 1 mM on freshly cleaved V1 grade mica surface for 30 min in a closed humid chamber. After deposition, images of samples were recorded under phosphate buffer inside an AFM liquid chamber. The relatively high concentration of FPF and FPF-F6 was chosen to encourage their self-assembly. Figure 7 shows the resulting images. In the case of FPF, one observes fiberlike structures that densely adsorb onto the mica surface. FPF-F6 instead forms spherically shaped nanoparticles, and the surface coverage is less pronounced. The size and aspect ratio of the aggregates reflect that the optimal intermolecular packing geometries for minimizing the π -component contact with water for the two molecular systems are different. We recognize that binding to the negatively charged mica may perturb the general physical characteristics of the supramolecular structures. For example, aggregates on mica may favor a curvature lower than the corresponding free species. Mica may also allow closer packing of oppositely charged terminal groups at the surface than is found in free micelles, since the surface acts as a highly charged laterally extended counterion.^[18] Despite these uncertainties, the data in Figure 7 highlight that the final structures of the aggregates and ability of conjugated oligoelectrolytes to bind to oppositely charged macromolecules or surfaces is heavily influenced by the internal molecular features of the conjugated framework; such considerations are of particular importance for situations in which selective binding to charged surfaces is an important part of the sensory process, for example, in DNA chips.^[19]

Photophysics of electrostatic aggregates: Electrostatic binding of cationic COEs to negatively charged macromolecules induces electrostatic complexation and the formation of inter-oligoelectrolyte aggregates.^[2] While the spectral properties of such nanoheterogeneous systems provide the basis for transduction,^[20] for example, in protein identification assays,^[2] the effect of local structure on the basic optical features of the COEs remains unexplored. Conversely, introducing molecules within these higher-order supramolecular systems can be used to gain insight into the basic characteristics of optical reporters. For the studies reported herein, we examined how FPF and FPF-F6 interact with negatively charged ssDNA in dilute phosphate buffer. The randomly chosen ssDNA sequence corresponds to 5'-TGA CCA ACC ACA CCA ACC-3'. The COE/ssDNA stoichiometry was

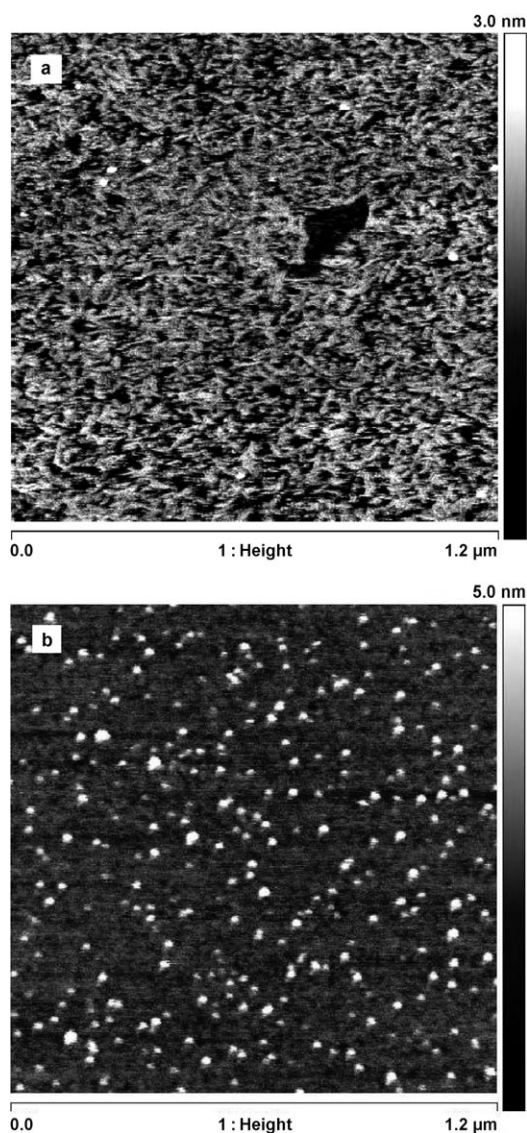


Figure 7. Imaging of the aggregates of a) fiberlike FPF and b) spherically shaped nanoparticles of FPF-F6 by using solution AFM. All images were collected in the scale of $1.2 \times 1.2 \mu\text{m}$, the images represent height channel (the z scale corresponds to 10 nm).

calculated based on the ratio of positive and the negative charges.

Figure 8 compares the absorption spectra of FPF and FPF-F6 in the absence and presence of ssDNA. The absorption maxima of FPF remain relatively unperturbed. However, in the case of FPF-F6 one observes the appearance of a redshifted shoulder when ssDNA is present. Figure 9 shows that the PL spectra of FPF-F6 blueshifts in the presence of the ssDNA. No such changes occur for FPF (see the Supporting Information). Therefore, at least in the case of FPF-F6, complexation to ssDNA yields a redshift in absorption and a blueshift in emission. The former we attribute to structural modification of the π system when incorporated into the aggregate, for example, a more coplanar arrangement of the aromatic units, which would increase the effective

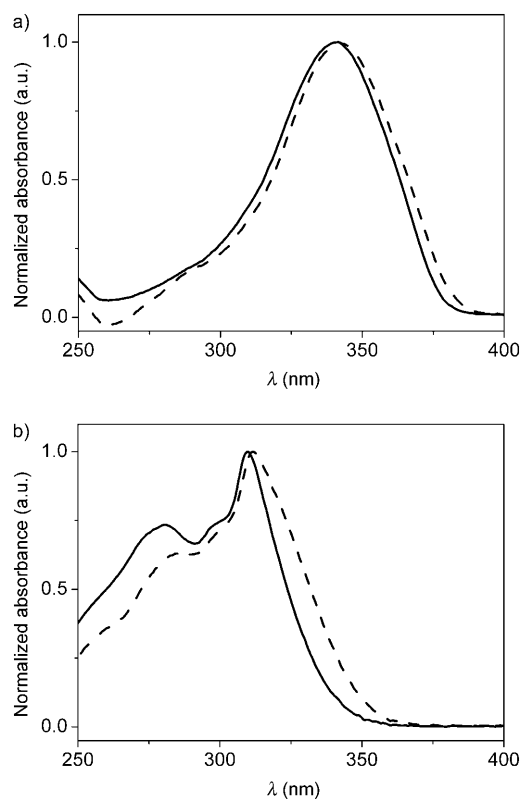


Figure 8. Absorption spectra of a) FPF/ssDNA and b) FPF-F6/ssDNA in phosphate buffer with the ratio of positive to negative charge $R_{+/-}=0.26$ (dashed lines). The solid line is the spectrum without ssDNA shown for ease of comparison. The concentration of the oligomers is $5 \mu\text{M}$.

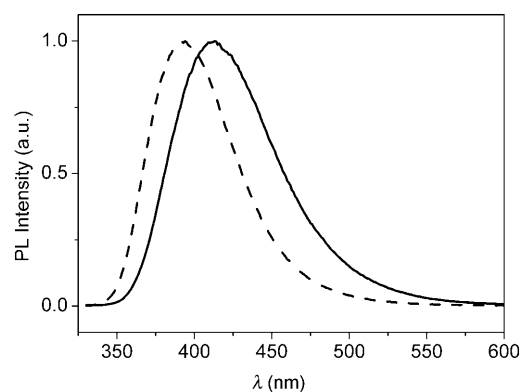


Figure 9. PL spectra of FPF-F6/ssDNA (dashed line) in phosphate buffer with the positive to negative charge ratio $R_{+/-}=0.26$. Shown in a solid black line is the spectrum without ssDNA for comparison.

tive electronic delocalization. The emission at higher energies is attributed to increased hydrophobic contacts within the inter-oligoelectrolyte aggregates, which decreases the ability of water to stabilize the charge-transfer excited state.

Conclusion

We report on the synthesis and characterization of FPF-F6, a new COE that contains bulky trifluoromethyl substituents

on a central phenylene unit flanked by two fluorene fragments. The optical properties of this molecule reveal features as a result of steric constraints that disfavor a coplanar arrangement of the aromatic units in the ground state and therefore minimize π delocalization. However, the strong solvatochromic dependence of the PL emission indicates an excited state with substantial intramolecular charge-transfer character. We propose that excitation leads to a planarization of the molecule and that this geometry favors intramolecular charge transfer, wherein the outer fluorene units take up the role of donor units and the internal, electron-poor unit behaves as the acceptor site. The overall process is summarized in Scheme 2.

Structural characterization of the precursor molecules p-FPF and p-FPF-F6 confirm the higher torsional angle between aromatic segments. Furthermore, the lattice arrangement shows much weaker interactions for the fluorinated species. It is tempting to assume that the tighter π - π contacts in the precursor p-FPF molecule are also present in the hydrophobic aggregates of FPF, and that this feature is responsible for the fiberlike aggregates observed by solution AFM. The difference in intramolecular arrangements and steric substitution not only influences the shape of these aggregates, but also their ability to bind to oppositely charged species. This latter point is demonstrated by the lower density of FPF-F6 aggregates imaged on mica; see Figure 7a and b. It is also worth noting the relevance to biosensory assays that depend on the electrostatic binding of reporter COEs upon specific biomolecular recognition events, as for instance hybridization of complementary ssDNA to neutral PNA-containing surfaces.^[19]

Monitoring the absorbance of FPF-F6 to ssDNA reveals that the absorption is redshifted, which we take to indicate that the association between oppositely charged groups has an influence on the conformation of the π -conjugated segment. These conditions appear to lead to a less twisted internal conformation. Furthermore, that the PL spectra of FPF-F6 displays a solvatochromic effect due to the charge-trans-

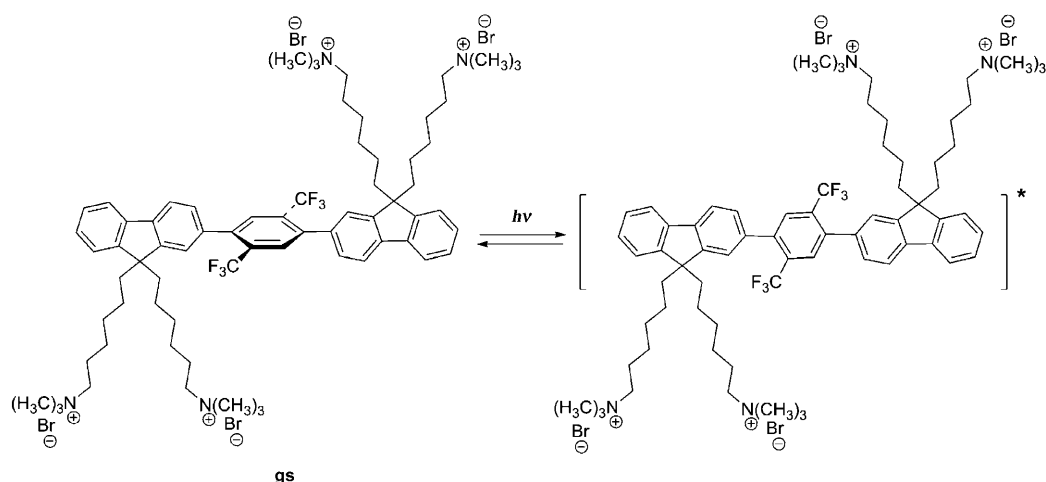
fer characteristics allows one to establish that the chromophores in the ssDNA oligoelectrolyte aggregates find themselves in a much less polar environment, relative to the situation when they are dissolved in buffer. While the internal structure of these electrostatic aggregates is unknown at this point, the data indicate that not only is charge pairing significant, but also interactions between the hydrophobic components, which ultimately are capable of effectively shielding the optical units from contact with water.

Findings described herein highlight that significant complexity can be found even in the most basic optical properties and supramolecular structures of COEs. A better understanding of the myriad processes involved in determining the final optical response provides a better rationale for incorporation of these emerging materials within technologies associated with biosensors and optoelectronic devices.

Experimental Section

General: Unless otherwise indicated, all reagents were obtained from commercial suppliers (Sigma-Aldrich, Acros), of which *N*-bromosuccinimide (NBS) was used after recrystallization in hot water, whereas other chemicals were used without further purification. ^1H and ^{13}C NMR spectra were collected on a Varian UNITY INOVA 400 MHz NMR spectrometer. Mass spectroscopy and elemental analysis were performed in the UC Santa Barbara Mass Spectrometry Lab and Elemental Analysis Center. TGA measurements were finished in Materials Research Laboratory, UC Santa Barbara, by using a Mettler TGA/SDTA851e thermogravimetric analyzer. UV spectra were recorded on a Shimadzu UV-2401 PC diode array spectrometer. Fluorescence spectra were recorded using a Spex Fluorolog 2 spectrometer equipped with a xenon lamp light source and photomultiplier tube detector.

Liquid-phase AFM images: The AFM images were recorded in the amplitude-modulated tapping mode by using a MultiMode microscope equipped with an E scanner controlled by Nanoscope IIIA (Veeco, Santa Barbara, CA). For experiments performed under liquid, a new type of silicon nitride probes (MSNL-Au coated) with a resonance frequency of approximately 8 kHz and a spring constant of $k \approx 0.03 \text{ N m}^{-1}$ (Veeco Probes, Santa Barbara, CA) were used. Images were processed and analyzed by using NanoScope software (Veeco, Santa Barbara, CA) and leveled by a first-order plane fit to correct for the sample tilt.



Scheme 2. Schematic illustration of the geometry transition of FPF-F6 from a twisted ground state (gs) to a planar excited state (*).

Single-crystal structural analysis: The crystal was mounted on a glass fiber and transferred to a Bruker CCD platform diffractometer. The SMART program was used to determine the unit cell parameters and data collection (25 s per frame, 0.3° per frame for a sphere of diffraction data).^[21] The data were collected at 220 K by using an Oxford nitrogen gas cryostream system. The raw frame data were processed by using the SAINT program.^[22] The empirical absorption correction was applied based on psi-scan. Subsequent calculations were carried out by using the SHELXTL program.^[23]

Compound 1: ¹H NMR (400 MHz, CDCl₃): δ = 0.55–0.60 (m, 4H), 1.03–1.09 (m, 4H), 1.13–1.21 (m, 4H), 1.40 (s, 12H), 1.6–1.67 (m, 4H), 1.96–2.02 (m, 4H), 3.25–3.29 (t, *J* = 7.0, 4H), 7.33–7.36 (m, 3H), 7.70–7.75 (m, 3H), 7.80–7.83 ppm (d, *J* = 7.6, 1H); elemental analysis calcd (%) for C₃₁H₄₃BBr₂O₂: C 60.36, H 6.92; found: C 60.68, H 6.93.

Compound 2: ¹H NMR (400 MHz, CDCl₃): δ = 8.01 ppm (s, 2H).

Compound p-FPF-F6: Compounds **1** (7.096 g, 11.29 mmol), **2** (2 g, 5.38 mmol), and [Pd(PPh₃)₄] (130 mg) were added to a solution of toluene (50 mL) and 2 M K₂CO₃ (26.9 mL). The mixture was vigorously stirred at 95 °C for 24 h under an argon atmosphere. The mixture was cooled to room temperature. CH₂Cl₂ was used to extract the product, which was then washed with brine and water, and dried with anhydrous MgSO₄. The crude product was obtained by removing the solvent under vacuum; this was then purified by chromatography on a silica gel column using 3:1 (v/v) hexane/CH₂Cl₂ as the eluent to give p-FPF-F6 as colorless crystal (2.9 g, 45%). ¹H NMR (400 MHz, CDCl₃): δ = 0.66–0.67 (m, 8H), 1.08–1.14 (m, 8H), 1.18–1.26 (m, 8H), 1.64–1.71 (m, 8H), 1.99–2.04 (t, *J* = 8.2, 8H), 3.28–3.31 (t, *J* = 7.0, 8H), 7.36–7.39 (m, 10H), 7.76–7.81 (m, 4H), 7.86 ppm (s, 2H); ¹³C NMR (400 MHz, CDCl₃): δ = 23.7, 28.0, 29.2, 32.8, 34.2, 40.5, 55.4, 111.5, 119.7, 120.3, 122.3, 123.1, 123.8, 125.1, 127.3, 127.8, 127.9, 130.3, 131.3, 131.6, 137.1, 140.7, 141.3, 141.6 ppm; MS (FAB/NBA): *m/z*: 1190–1198; elemental analysis calcd (%) for C₅₈H₆₄Br₄F₆: C 58.48, H 5.38; found: C 58.43, H 5.36.

Compound PF6-F6: p-FPF-F6 (119 mg, 0.1 mmol) was dissolved in THF (15 mL). Condensed trimethylamine (2 mL) was added dropwise under a slight vacuum to the solution at –78 °C. After that, the mixture was gradually warmed to room temperature with stirring overnight. A colorless precipitate was observed. After methanol (30 mL) was added to dissolve this precipitate, additional trimethylamine (1.5 mL) was added at –78 °C. The mixture was vigorously stirred for another 24 h. The solvent was removed under vacuum. The residue was washed with hexane and acetone sequentially, and dried in vacuo. PF6-F6 was obtained as white solid (126 mg, 89%). TGA showed that one mole of molecule co-crystallized with seven moles of water. ¹H NMR (400 MHz, CD₃OD): δ = 0.60–0.73 (m, 8H), 1.13–1.21 (m, 8H), 1.56–1.64 (m, 8H), 2.08–2.14 (m, 8H), 3.07 (s, 36H), 3.20–3.25 (m, 8H), 7.38–7.41 (m, 6H), 7.46–7.49 (m, 4H), 7.83–7.90 (m, 6H), 7.90 ppm (s, 2H); ¹³C NMR (400 MHz, CD₃OD): δ = 26.4, 27.5, 29.7, 33.1, 43.9, 56.2, 59.1, 70.4, 123.4, 123.9, 126.4, 126.8, 127.5, 129.1, 131.1, 133.9, 134.9, 135.2, 140.9, 144.7, 145.5, 145.8, 154.1, 154.6; MS (ESI-MS): *m/z*: 277 [M–4Br]⁴⁺.

Acknowledgements

The authors are grateful to the DOE and the ICB for financial support, to Dr. Huaping Li for providing the compounds p-FPF and PF6, to Dr. Arkadiusz Chworos for liquid-phase AFM measurements, to Dr. Gang Wu for assistance with the crystallographic studies, and to Alexander Mikhailovsky for help on spectra measurements. Y.R. thanks the financial supports of the State National Natural Science Foundation of China (grant no. 50603011) and China Scholarship Council.

- [1] R. Q. Yang, Y. H. Xu, X. D. Dang, T. Q. Nguyen, Y. Cao, G. C. Bazan, *J. Am. Chem. Soc.* **2008**, *130*, 3282–3283.
- [2] H. P. Li, G. C. Bazan, *Adv. Mater.* **2009**, *21*, 964–967.
- [3] Y. H. Xu, R. Q. Yang, J. B. Peng, A. Mikhailovsky, Y. Cao, T. Q. Nguyen, G. C. Bazan, *Adv. Mater.* **2009**, *21*, 584–588.

- [4] C. V. Hoven, A. Garcia, G. C. Bazan, T. Q. Nguyen, *Adv. Mater.* **2008**, *20*, 3793–3810.
- [5] a) H. Jiang, P. Taranekekar, J. R. Reynolds, K. S. Schanze, *Angew. Chem.* **2009**, *121*, 4364–4381; *Angew. Chem. Int. Ed.* **2009**, *48*, 4300–4316; b) B. S. Gaylord, A. J. Heeger, G. C. Bazan, *Proc. Natl. Acad. Sci. USA* **2002**, *99*, 10954–10957; c) D. L. Wang, X. Gong, P. S. Heeger, F. Rininsland, G. C. Bazan, A. J. Heeger, *Proc. Natl. Acad. Sci. USA* **2002**, *99*, 49–53; d) J. Tian, C. C. Wu, M. E. Thompson, J. C. Sturm, R. A. Register, *Chem. Mater.* **1995**, *7*, 2190–2198; e) A. F. Thünemann, *Adv. Mater.* **1999**, *11*, 127–130; f) T. Kawai, T. Yamaue, K. Tada, M. Onoda, S. H. Jin, S. K. Choi, K. Yoshino, *Jpn. J. Appl. Phys. Part 2* **1996**, *35*, L741–L744; g) V. Cimrová, W. Schmidt, R. Rulkens, M. Schulze, W. Meyer, D. Neher, *Adv. Mater.* **1996**, *8*, 585–588.
- [6] a) *Self-Assembling Complexes for Gene Delivery. From Laboratory to Clinical Trial* (Eds.: A. V. Kabanov, P. Felgner, L. W. Seymour), Wiley, New York, **1998**; b) M. Stork, B. S. Gaylord, A. J. Heeger, G. C. Bazan, *Adv. Mater.* **2002**, *14*, 361–366; c) J. W. Hong, W. L. Henne, G. E. Keller, M. T. Rinke, G. C. Bazan, *Adv. Mater.* **2006**, *18*, 878–882; d) C. Chi, A. Mikhailovsky, G. C. Bazan, *J. Am. Chem. Soc.* **2007**, *129*, 11134–11145; e) J. G. Müller, E. Atas, C. Tan, K. S. Schanze, V. D. Kleiman, *J. Am. Chem. Soc.* **2006**, *128*, 4007–4016; f) R. Q. Yang, H. B. Wu, Y. Cao, G. C. Bazan, *J. Am. Chem. Soc.* **2006**, *128*, 14422–14423.
- [7] a) C. Y. Tan, M. R. Pinto, K. S. Schanze, *Chem. Commun.* **2002**, 446–447; b) H. Schnablegger, M. Antonietti, C. Goltner, J. Hartmann, H. Colfen, P. Samori, J. P. Rabe, H. Hager, W. Heitz, *J. Colloid Interface Sci.* **1999**, *212*, 24–32; c) K. Y. Pu, L. P. Cai, B. Liu, *Macromolecules* **2009**, *42*, 5933–5940; d) P. Björk, D. Thomsson, O. Mirzov, J. Wigenius, O. Inganäs, I. G. Scheblykin, *Small* **2009**, *5*, 96–103; e) C. Y. Tan, E. Atas, J. G. Müller, M. R. Pinto, V. D. Kleiman, K. S. Schanze, *J. Am. Chem. Soc.* **2004**, *126*, 13685–13694; f) H. Jiang, X. Y. Zhao, K. S. Schanze, *Langmuir* **2007**, *23*, 9481–9486; g) J. Kim, T. M. Swager, *Nature* **2001**, *411*, 1030–1034; h) M. R. Pinto, B. M. Kristal, K. S. Schanze, *Langmuir* **2003**, *19*, 6523–6533; i) C. Y. Tan, M. R. Pinto, M. Erkan Kose, I. Ghiviriga, K. S. Schanze, *Adv. Mater.* **2004**, *16*, 1208–1212.
- [8] F. J. M. Hoebe, P. Jonkheijm, E. W. Meijer, A. P. H. Schenning, *Chem. Rev.* **2005**, *105*, 1491–1546.
- [9] B. Liu, B. S. Gaylord, S. Wang, G. C. Bazan, *J. Am. Chem. Soc.* **2003**, *125*, 6705–6714.
- [10] S. Wang, B. Liu, B. S. Gaylord, G. C. Bazan, *Adv. Funct. Mater.* **2003**, *13*, 463–467.
- [11] J. H. Ortony, R. Yang, J. Z. Brzezinski, L. Edman, T.-Q. Nguyen, G. C. Bazan, *Adv. Mater.* **2008**, *20*, 298–302.
- [12] a) J. W. Hong, H. Y. Woo, B. Liu, G. C. Bazan, *J. Am. Chem. Soc.* **2005**, *127*, 7435–7443; b) S. J. K. Pond, O. Tsutsumi, M. Rumi, O. Kwon, E. Zojer, J.-L. Brédas, S. R. Marder, J. W. Perry, *J. Am. Chem. Soc.* **2004**, *126*, 9291–9306.
- [13] J. N. Wilson, M. Josowicz, Y. Q. Wang, Uwe H. F. Bunz, *Chem. Commun.* **2003**, 2962–2963.
- [14] J. R. Lakowicz, *Principles of Fluorescence Spectroscopy*, Springer, Singapore, **2006**.
- [15] a) P. S. Sardar, S. S. Maity, L. Das, S. Ghosh, *Biochemistry* **2007**, *46*, 14544–14556; b) H. Inoue, T. Mori, T. Sakurai, *Chem. Lett.* **1980**, 683–686.
- [16] a) S. Wang, B. S. Gaylord, G. C. Bazan, *Adv. Mater.* **2004**, *16*, 2127–2132; b) O. K. Nag, M. Kang, S. Hwang, H. Suh, H. Y. Woo, *J. Phys. Chem. B* **2009**, *113*, 5788–5793; c) Y. Jin, R. Yang, H. Suh, H. Y. Woo, *Macromol. Rapid Commun.* **2008**, *29*, 1398–1402; d) G. C. Bazan, *J. Org. Chem.* **2007**, *72*, 8615–8635; e) B. Liu, G. C. Bazan, *J. Am. Chem. Soc.* **2006**, *128*, 1188–1196.
- [17] a) J. K. H. Horber, M. J. Miles, *Science* **2003**, *302*, 1002–1005; b) H. G. Hansma, J. Vesenska, C. Siegler, G. Kelderman, H. Morrett, R. L. Sinsheimer, V. Elings, C. Bustamante, P. K. Hansma, *Science* **1992**, *256*, 1180–1184; c) A. Chworos, I. Severcan, A. Y. Koyfman, P. Weinkam, E. Oroudjev, H. G. Hansma, L. Jaeger, *Science* **2004**, *306*, 2068–2072; d) B. Drake, C. B. Prater, A. L. Weisenhorn, S. A. Gould, T. R. Albrecht, C. F. Quate, D. S. Cannell, H. G.

- Hansma, P. K. Hansma, *Science* **1989**, *243*, 1586–1589; e) H. G. Hansma, L. Pietrasanta, *Curr. Opin. Chem. Biol.* **1998**, *2*, 579–584; f) S. Manne, J. P. Cleveland, H. E. Gaub, G. D. Stucky, P. K. Hansma, *Langmuir* **1994**, *10*, 4409–4413.
- [18] S. Manne, T. E. Schäffer, Q. Huo, P. K. Hansma, D. E. Morse, G. D. Stucky, I. A. Aksay, *Langmuir* **1997**, *13*, 6382–6387.
- [19] B. Liu, G. C. Bazan, *Proc. Natl. Acad. Sci. USA* **2005**, *102*, 589–593.
- [20] a) X. L. Feng, X. R. Duan, L. B. Liu, F. D. Feng, S. Wang, Y. L. Li, D. B. Zhu, *Angew. Chem.* **2009**, *121*, 5420–5425; *Angew. Chem. Int. Ed.* **2009**, *48*, 5316–5321; b) F. Pu, Z. Huang, D. Hu, J. Ren, S. Wang, X. Qu, *Chem. Commun.* **2009**, 7357–7359; c) F. Feng, F. He, L. An, S. Wang, Y. Li, D. B. Zhu, *Adv. Mater.* **2008**, *20*, 2959–2964; d) K. P. R. Nilsson, P. Hammarström, *Adv. Mater.* **2008**, *20*, 2639–2645; e) K. P. R. Nilsson, A. Herland, P. Hammarström, O. Inganäs, *Biochemistry* **2005**, *44*, 3718–3724.
- [21] SMART Software Users Guide, Version 5.1, Bruker AXS, Inc., Madison, Wisconsin, **1999**.
- [22] SAINT Software Users Guide, Version 5.1, Bruker AXS, Inc., Madison, Wisconsin (USA), **1999**.
- [23] SHELXTL, Version 6.12, G. M. Sheldrick, Bruker AXS, Inc., Madison, Wisconsin (USA), **2001**.

Received: April 8, 2010
Published online: August 16, 2010